International Journal of Heat and Mass Transfer 53 (2010) 3887–3897

Contents lists available at ScienceDirect

International Journal of Heat and Mass Transfer

journal homepage: www.elsevier.com/locate/ijhmt

# Enhancement of forced convection heat transfer in a three-dimensional laminar channel flow with insertion of a moving block

Wu-Shung Fu *, Jieh-Chau Huang, Chung-Gang Li

*Department of Mechanical Engineering, National Chiao Tung University, Hsinchu 30010, Taiwan, ROC*

ARTICLE INFO

*Article history:*
Received 9 March 2010
Received in revised form 16 April 2010
Accepted 16 April 2010
Available online 9 June 2010

*Keywords:*
Forced convection
Channel flow
Compressible flow
Immersed boundary
Moving boundary

ABSTRACT

Enhancement of heat transfer rate of a heat surface in a three-dimensional channel flow with insertion of a moving slender block is investigated numerically. A slender block is installed along the direction of the channel flow, and the movement of the slender block is in periodic motion and transverse to the channel flow. Due to the interaction between the channel flow and slender block moving, a large circulation vertical to the channel flow is induced and follows the moving slender block closely. The behaviors of the slender block and circulation destroy and suppress the velocity and thermal boundary layers on the heat surface periodically. These phenomena first observed cause the heat transfer rate of the heat surface to be enhanced especially in the downstream of the heat surface. The maximum magnitude of enhancement in this study is about 50%.



## 1. Introduction

Until now a problem of forced convection of a heat surface in a channel flow is usually of practical importance, and widely considered in the design of devices such as heat exchangers, nuclear reactors, and solar energy systems. Thus, an effective method for improving the heat transfer performance of forced convection in the channel flow is urgently expected.

In the past, Bergles [1,2] had reviewed the development in convective heat transfer augmentation in detail and related studies are continued to be investigated up to now. At present well-known methods of the enlargement of heat dissipation surface [3–11], the disturbance of flow field [12–19] and the vibration of heat surface [20–26] are most usually adopted to enhance the forced convection heat transfer rate of the channel flow and the results of the above methods are remarkable and available. However, the increment of the heat transfer rate of the above methods seems to have limitation because a thermal boundary layer which is disadvantageous to heat transfer mechanisms still forms on the heat surface. Therefore, Fu et al. [27,28] proposed a new method in which the thermal boundary layer forming on the heat plate was destroyed periodically by a block moving back and forth on the heat plate to enhance the heat transfer rate of the heat plate, and remarkable heat transfer rates were achieved. The situation investigated numerically and experimentally in the above studies was a heat surface under a two-dimensional slot jet flow. It is well-known that the jet flow has a superior heat transfer rate in the whole region, but in the channel flow the heat transfer rate of the heat surface varies drastically from excellent to low level along the flow direction. Then, using a block moving periodically on the whole heat surface to improve the heat transfer rate of the heat surface in the channel flow, especially in the downstream region, can yet be regarded as an available method.

Therefore, the aim of this study investigates the forced convection heat transfer rate of the heat surface in a channel flow enhanced by a moving block numerically. The moving block of which the movement is transverse to the channel flow and moves periodically back and forth on the heat surface is installed along the channel flow direction. Since the moving direction of the block is vertical to the channel flow direction, the geometrical situation becomes a three-dimensional model. To avoid the necessity of a huge memory in three-dimensional computation processes, the immersed boundary method based on a finite difference scheme developed by Peskin [29] substituting the Arbitrary Largrangian–Eulerian method of finite element scheme used in the previous study [27] is adopted. The movement of the block causes the spaces distributed in both sides of the block to be contracted and enlarged simultaneously. The compressibility of fluid is then considered. In addition, requisite methods of Roe scheme, preconditioning, and dual-time-stepping available for compressible fluid flows are adopted to resolve the governing equations. The results show that under high velocities of the channel flow and block situations, the superior enhancements of heat transfer rates are

* Corresponding author. Address: Department of Mechanical Engineering, National Chiao Tung University, 1001 Ta Hsueh Road, Hsinchu 30056, Taiwan, ROC. Tel.: +886 3 5712121x55110; fax: +886 3 5720634.
*E-mail address:* wsfu@mail.nctu.edu.tw (W.-S. Fu).

0017-9310/$ - see front matter © 2010 Elsevier Ltd. All rights reserved.
doi:10.1016/j.ijheatmasstransfer.2010.05.007

**Nomenclature**

| | |
|---|---|
| $En$ | enhancement of the average heat transfer rate of the heat surface of a cycle in Eq. (32) |
| $g$ | acceleration of gravity (m/s$^2$) |
| $h$ | dimensional height of the slender block (m) |
| $k$ | thermal conductivity (W/mK) |
| $l_1$ | dimensional length of the channel (m) |
| $l_2$ | dimensional length of the slender block (m) |
| $l_3$ | the distance between the inlet and the heat surface (m) |
| $l_4$ | the distance between the outlet and the heat surface (m) |
| $M$ | local Mach number |
| $Nu_{X_1}$ | Nusselt number defined in Eq. (27) |
| $Nu_{X_3}$ | Nusselt number defined in Eq. (7b) |
| $\overline{Nu}$ | average Nusselt number defined in Eq. (30) |
| $\overline{Nu}_{X_1}$ | average Nusselt number defined in Eq. (31) |
| $(Nu)$ | average Nusselt number defined in Eq. (32) |
| $R$ | gas constant (J/kg/K) |
| Re | Reynolds number defined in Eq. (7a) |
| $t$ | time (s) |
| $T$ | temperature (K) |
| $T_0$ | temperature of surroundings (K) |
| $T_f$ | film temperature (K) |
| $T_h$ | temperature of heat surface (K) |
| $u_1, u_2, u_3$ | velocities in $x_1$, $x_2$ and $x_3$ directions (m/s) |
| $U_1, U_2, U_3$ | dimensionless velocities in $X_1$, $X_2$ and $X_3$ directions |
| $v_b$ | moving velocity of the slender block (m/s) |
| $V_b$ | dimensionless velocity of the slender block |
| $w_1$ | dimensional width of the channel (m) |
| $w_2$ | dimensional height of the channel (m) |
| $w_3$ | dimensional width of the slender block (m) |
| $x, y, z$ | Cartesian coordinates (m) |
| $X_1, X_2, X_3$ | dimensionless Cartesian coordinates |

*Greek symbols*

| | |
|---|---|
| $\gamma$ | specific heat ratio |
| $\xi, \eta, \zeta$ | curvilinear coordinates |
| $\theta$ | dimensionless temperature |
| $\mu$ | viscosity (N s/m$^2$) |
| $\mu_0$ | Surrounding viscosity (N s/m$^2$) |
| $\rho$ | density (kg/m$^3$) |
| $\rho_0$ | surrounding density (kg/m$^3$) |

achieved and the maximum enhancement is about 50%. However, under low velocities of the channel flow and block situations, the behavior of the block oppositely becomes a burden which causes the enhancement of heat transfer rate to be dulled and even a counter-effect is observed.

## 2. Physical model

The physical model investigated in this study is a three-dimensional situation and shown in Fig. 1. The width, height, and length of the channel are $w_1$, $w_2$, and $l_1$, respectively. A heat surface ABDC of which the width, length, and temperature are $w_1$, $l_2$, and $T_h$, respectively, is installed on the bottom surface. The distances from the inlet and outlet to the heat surface are $l_3$ and $l_4$, respectively. Cooling fluid flows into the channel, and the uniform velocity and temperature of the cooling fluid are $u_0$ and $T_0$, respectively. The thermal and flowing conditions of the cooling fluid at the outlet are fully developed. A moving slender block which has width $w_3$, length $l_2$, and height $h$ is set on the heat surface. In order to avoid the impediment of channel flow in the regions near both vertical walls, the slender block moves at the constant speed of $v_b$ from the point of $p_r$ to the point of $p_l$, and the distances from the right and left walls to the points of $p_r$ and $p_l$ are the same and equal to $\frac{1}{4}w_1$. The purpose of the moving slender block is to destroy the thermal boundary layer forming on the heat surface, and then the height of the moving block is higher than the thickness of the thermal boundary layer. Except the heat surface, the other surfaces including the moving slender block are adiabatic. The laminar forced convection is studied exclusively in this work, and the effects of turbulence and gravity on the heat transfer mechanisms of the heat surface are neglected. According to Trong [30], the governing equations are expressed as follows:

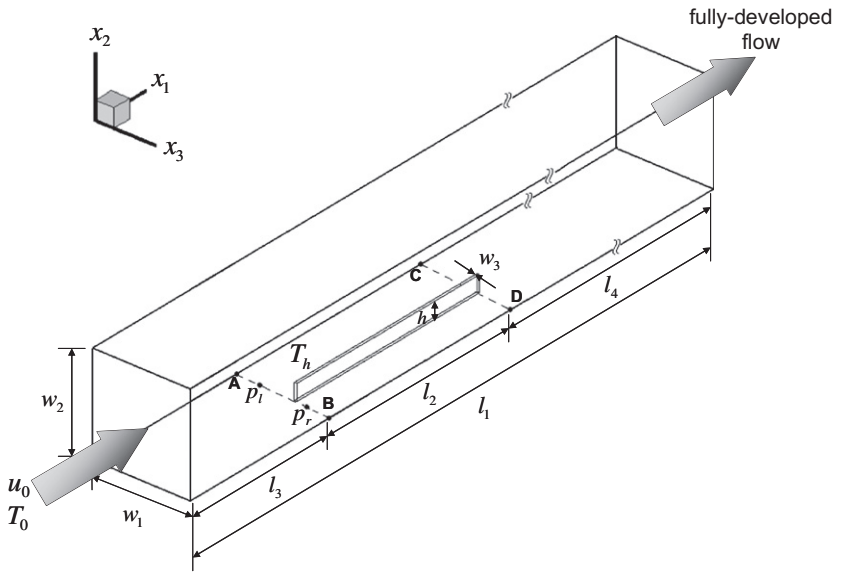


**Fig. 1.** Physical model.

$$\frac{\partial U}{\partial t}+\frac{\partial F_1}{\partial x_1}+\frac{\partial F_2}{\partial x_2}+\frac{\partial F_3}{\partial x_3}=0 \tag{1}$$

The quantities included in $U$ and $F_i$ are separately shown in the following equations:

$$U=\begin{pmatrix}\rho\\ \rho u_1\\ \rho u_2\\ \rho u_3\\ \rho e\end{pmatrix} \tag{2}$$

and

$$F_i=\begin{pmatrix}\rho u_i\\ \rho u_i u_1+P\delta_{i1}-\mu A_{i1}\\ \rho u_i u_2+P\delta_{i2}-\mu A_{i2}\\ \rho u_i u_3+P\delta_{i3}-\mu A_{i3}\\ (\rho e+P)u_i-\mu A_{ij}u_j-\lambda\frac{\partial T}{\partial x_i}\end{pmatrix},\quad \forall i=1,2,3 \tag{3}$$

where $A_{ij}=\frac{\partial u_j}{\partial x_i}+\frac{\partial u_j}{\partial x_i}-\frac{2}{3}(\nabla\cdot u)\delta_{ij}$ and the ideal gas equation is written by

$$P=\rho RT \tag{4}$$

The Sutherland's law is adopted to evaluate the viscosity and the thermal conductivity as follows:

$$\mu(T)=\mu_0\left(\frac{T}{T_0}\right)^{\frac{2}{3}}\frac{T_0+110}{T+110} \tag{5}$$

$$k(T)=\frac{\mu(T)\gamma R}{(\gamma-1)\mathrm{Pr}}$$

where $\rho_0$ = 1.1842 kg/m$^3$, $\mu_0 = 1.85\times10^{-5}$ N s/m$^2$, $T_0$ = 298.0592 K, $\gamma$ = 1.4, $R$ = 287 J/kg/K and Pr = 0.72 .

To simplify the analysis of results, the following dimensionless variables are made.

$$X_1=\frac{x_1}{w_1},\quad X_2=\frac{x_2}{w_1},\quad X_3=\frac{x_3}{w_1}$$

$$U_1=\frac{u_1}{u_0},\quad U_2=\frac{u_2}{u_0},\quad U_3=\frac{u_3}{u_0},\quad V_b=\frac{v_b}{u_0} \tag{6}$$

The compressibility and viscosity of the working fluid are considered, and the definition of the Reynolds number Re and the local Nusselt number $Nu_{x_3}$ on a certain $x_2x_3$ cross section of the heat surface is defined as follows:

$$\mathrm{Re}=\frac{\rho_0 u_0 w_1}{\mu_0} \tag{7a}$$

$$Nu_{X_3}=\frac{w_1}{k_0(T_h-T_0)}\left[k(T)\frac{\partial T}{\partial x_2}\right] \tag{7b}$$

Since the conditions of the channel flow are dynamic and unsteady throughout, in Eq. (7b) the temperature difference of $(T_h-T_f)$ which is usually used in a convection channel flow is conveniently substituted by $(T_h-T_0)$ .

## 3. Numerical method

Accompanying with the usage of Roe and preconditioning methods [31], two other effective methods are used together to avoid the occurrence of inefficiency and inaccuracy in computing processes. One is the method of three-dimensional curvilinear coordinate $(\xi,\eta,\zeta)$ to be used for clustering the grids near the heat surface. A dual-time-stepping process is the other one to improve the efficiency of convergence. The original governing Eq. (1) is then transformed into the following equation:

$$\Gamma\frac{\partial U_p}{\partial\tau}+\frac{\partial U}{\partial t}+\frac{\partial F_1}{\partial\xi}+\frac{\partial F_2}{\partial\eta}+\frac{\partial F_3}{\partial\zeta}=0 \tag{8}$$

where $\Gamma$ is the preconditioning matrix derived by Weiss and Smith [32], and $U_p$ is the primitive form $[P,u_1,u_2,u_3,T]/J$ in which $J$ is Jacobian matrix. $\tau$ and $t$ are the artificial and physical times, respectively, and $U$ is the conservative form of $(\rho,\rho u_1,\rho u_2,\rho u_3,\rho e)/J$. The preconditioning parameter $\beta$ according to Dennis et al. [33] is chosen as $\beta = max(\min(M^2,1.0),\beta_{\min})$, where $M$ is the local Mach number, and $\beta_{\min}\approx 3M_\infty^2$. $M_\infty$ is the approaching Mach number.

To discretize Eqs. (8) and (9) is obtained. The terms of $\frac{\partial U_p}{\partial\tau}$ and $\frac{\partial U}{\partial t}$ are differentiated by the first order forward difference and the second order backward difference, respectively, and the terms of $\frac{\partial F_1}{\partial\xi}$, $\frac{\partial F_2}{\partial\eta}$, and $\frac{\partial F_3}{\partial\zeta}$ are differentiated by the central difference.

$$\Gamma\frac{U_p^{k+1}-U_p^k}{\Delta\tau}+\frac{3U^{k+1}-4U^n+U^{n-1}}{2\Delta t}+\frac{1}{\Delta\xi}\left(F^{k+1}_{1_{i+\frac12,j,k}}-F^{k+1}_{1_{i-\frac12,j,k}}\right)+\frac{1}{\Delta\eta}\left(F^{k+1}_{2_{i,j+\frac12,k}}-F^{k+1}_{2_{i,j-\frac12,k}}\right)+\frac{1}{\Delta\zeta}\left(F^{k+1}_{3_{i,j,k+\frac12}}-F^{k+1}_{3_{i,j,k-\frac12}}\right)=0 \tag{9}$$

In which superscripts of $k$ and $n$ indicate the iteration numbers of artificial time and proceeding step of real time, respectively. When the term of artificial time $\frac{\partial U_p}{\partial\tau}$ is convergent to $\varepsilon(=10^{-3})$, Eq. (9) is automatically transferred into the Navier–Stokes equation and the values at the iteration number of $(k+1)$ of the artificial time in Eq. (9) substantially become the values at the proceeding step of $(n+1)$ of the real time.

Afterward the terms of $U^{k+1}$ and $F_i^{k+1}$ in Eq. (9) are necessary to be linearized and expressed as follows, respectively.

$$U^{k+1}=U^k+M\Delta U_p \tag{10}$$

where $M=\frac{\partial U}{\partial U_p}$ and $\Delta U_p=U_p^{k+1}-U_p^k$

$$F_1^{K+1}=F_1^K+A_p\Delta U_p \tag{11}$$

where $A_p=\frac{\partial F_1^k}{\partial U_p}$ is the flux Jacobian and the same method for $B_p=\frac{\partial F_2^k}{\partial U_p}$ and $C_p=\frac{\partial F_3^k}{\partial U_p}$ is used in linearization of $F_2^{K+1}$ and $F_3^{K+1}$, respectively.

To substitute Eqs. (10) and (11) into Eq. (9), the following equation is obtained.

$$\Gamma\frac{\Delta U_p}{\Delta\tau}+\frac{3(U^k+M\Delta U_p)-4U^n+U^{n-1}}{2\Delta t}+\delta_\xi(F_1^k+A_p\Delta U_p)+\delta_\eta(F_2^k+B_p\Delta U_p)+\delta_\zeta(F_3^k+C_p\Delta U_p)=0 \tag{12}$$

where $\delta_\xi$, $\delta_\eta$, and $\delta_\zeta$ are central-difference operators.

Eq. (12) can be rearranged as the following form:

$$\left[\Gamma\frac{I}{\Delta\tau}+M\frac{3}{2\Delta t}+(\delta_\xi A_p+\delta_\eta B_p+\delta_\zeta C_p)\right]\Delta U_p=R^k \tag{13}$$

where $R^k=-\left(\frac{3U^k-4U^n+U^{n-1}}{2\Delta t}\right)-(\delta_\xi F_1^k+\delta_\eta F_2^k+\delta_\zeta F_3^k)$, $I$ is the unit matrix.To divide the $\Gamma$ in both sides, the following equation is obtained.

$$\left[\frac{I}{\Delta\tau}+\Gamma^{-1}M\frac{3}{2\Delta t}+\Gamma^{-1}(\delta_\xi A_p^k+\delta_\eta B_p^k+\delta_\zeta C_p^k)\right]\Delta U_p=\Gamma^{-1}R^k \tag{14}$$

The solver of Eq. (15) is the LUSGS implicit method proposed by Yoon and Jameson [34] which is used to solve Eq. (14).

$$A_p=\Gamma^{-1}A_p^k$$

$$B_p=\Gamma^{-1}B_p^k \tag{15}$$

$$B_p=\Gamma^{-1}C_p^k$$

As for the computation of $R^k=-\left(\frac{3U^k-4U^n+U^{n-1}}{2\Delta t}\right)-(\delta_\xi F_1^k+\delta_\eta F_2^k+\delta_\zeta F_3^k)$ in RHS (right hand side) of Eq. (13), the terms of $F_i$ in Eq. (3) based on Cartesian coordinate can be divided into two parts. One is the inviscid term $F_{inviscid}$.

$$F_{inviscid} = \begin{pmatrix} \rho u_i \\ \rho u_i u_1 + P\delta_{i1} \\ \rho u_i u_2 + P\delta_{i2} \\ \rho u_i u_3 + P\delta_{i3} \\ (\rho e + P)u_i \end{pmatrix} \tag{16}$$

The other is viscous term $F_{viscous}$ .

$$F_{viscous} = -\begin{pmatrix} 0 \\ \mu A_{i1} \\ \mu A_{i2} \\ \mu A_{i3} \\ \mu A_{ij}u_j + \lambda \frac{\partial T}{\partial x_i} \end{pmatrix} \tag{17}$$

The upwind difference scheme developed by Roe [31] is employed in discretion of the term of $F_{inviscid}$ at the cells interface $(i+\frac{1}{2})$ and expressed as follows at low Mach number situation.

$$F_{inviscid,i+\frac{1}{2}} = \frac{1}{2}(F_R + F_L) - \frac{1}{2}\{|\Gamma^{-1}A_p|\Delta U_P\} \tag{18}$$

The fifth order MUSCL scheme proposed by Abalakin et al. [35] is used to compute the Eq. (18).

The derivative terms of $A_{ij} = \frac{\partial u_j}{\partial x_i} + \frac{\partial u_j}{\partial x_i} - \frac{2}{3}(\nabla \bullet u)\delta_{ij}$ in Eq. (17) are computed by the fourth order central difference.

$$\frac{\partial u}{\partial x} = \frac{u_{i-2} - 8u_{i-1} + 8u_{i+1} - u_{i+2}}{12\Delta x} + o(\Delta x^4) \tag{19}$$

The advantages of usage of LUSGS implicit method are to improve efficiency and decrease artificial dissipation.

The object of the study belongs to a kind of moving boundary problem and is appropriately resolved by two methods. One is the arbitrary Lagrangian and Eulerian method, and the other is the immersed boundary method. A three-dimensional compressible flow is considered, and then the immersed boundary method based on a finite difference scheme is adopted. The immersed boundary method was originally presented in the pioneering work of Peskin [29]. More recently, the application and simplified versions of the method were presented in [36–38]. According to the above literature, the Navier–Stokes equation with the force terms introduced through the boundary conditions can be written as follows:

$$\frac{\partial U}{\partial t} = -\left(\frac{\partial F_1}{\partial x_1} + \frac{\partial F_2}{\partial x_2} + \frac{\partial F_3}{\partial x_3}\right) + \rho F_B \tag{20}$$

where $F_B$ is the body force term computed at every time step, so that the velocity distribution on an arbitrary surface is equal to the function of $V_s$ .

$$U^{n+1} = U^n + \Delta t(Rhs + \rho F_B) = V_s \tag{21}$$

where *Rhs* includes all the pressure gradient, advection and diffusion terms. In case of a stationary solid body with no-slip boundary condition, the magnitude of $V_s$ is zero along the boundary. In this study, the specified velocity $V_s$ is equal to the velocity of the moving slender block. In order to lead the velocity of the next time step $U^{n+1}$ to be equal to the desired value $V_s$ on the immersed boundary, the source term $F_B$ of Eq. (20) can be expressed as follows [38]:

$$F_B = \frac{1}{\rho}\left(\frac{V_s - U^n}{\Delta t} - Rhs\right) \tag{22}$$

The main advantage of immersed boundary method is that the force $F_B$ can be prescribed on a regular grid, and the accuracy and efficiency of the solution procedure on simple rectilinear grids are maintained.

The adiabatic and no-slip conditions are adopted on the wall except for the heat surface. The equations are given as follows:

$$\begin{aligned} &P(i,0,k) = P(i,1,k) \\ &u_1(i,0,k) = -u_1(i,1,k) \\ &u_2(i,0,k) = -u_2(i,1,k) \\ &u_3(i,0,k) = -u_3(i,1,k) \\ &T(i,0,k) = T(i,1,k) \end{aligned} \tag{23}$$

The isothermal and no-slip conditions are adopted on the heat surface. The equations are given as follows:

$$\begin{aligned} &P(i,0,k) = P(i,1,k) \\ &u_1(i,0,k) = -u_1(i,1,k) \\ &u_2(i,0,k) = -u_2(i,1,k) \\ &u_3(i,0,k) = -u_3(i,1,k) \\ &T(i,0,k) = 2T_h - T(i,1,k) \end{aligned} \tag{24}$$

where $T_h$ is the wall temperature.

0 indicates the ghost cell and 1 indicates the cell most near the wall.

The uniform velocity at the inlet is $u_0$, and the fully-developed thermal and flow situations are obtained at the outlet. The inlet and outlet conditions can be expressed as the following equations, respectively.

$$\begin{aligned} &P(0,j,k) = 2P(1,j,k) - P(2,j,k) \\ &u_1(0,j,k) = u_0 \\ &u_2(0,j,k) = 0 \\ &u_3(0,j,k) = 0 \\ &T(0,j,k) = T_0 \end{aligned} \tag{25}$$

$$\begin{aligned} &P(nx+1,j,k) = P_{atm} \\ &u_1(nx+1,j,k) = u_1(nx,j,k) \\ &u_2(nx+1,j,k) = u_2(nx,j,k) \\ &u_3(nx+1,j,k) = u_3(nx,j,k) \\ &T(nx+1,j,k) = T(nx,j,k) \end{aligned} \tag{26}$$

where $P_{atm}$ is the atmosphere pressure with a constant of 101,300 Pa. 0 indicates the cell at the inlet and $nx+1$ indicates the cell at the outlet.

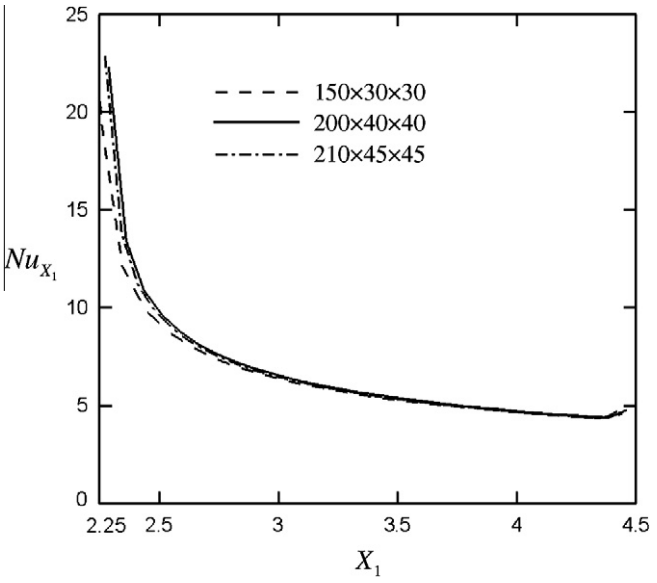


**Fig. 2.** Comparisons of local Nusselt number of heat surface along the centerline of streamwise direction. (Re=200)

## 4. Results and discussion

To obtain an optimal computation, three kinds of grid distributions are used to examine the adoptable grid distribution used in this study. The results of the distributions of the local Nusselt number $Nu_{X_1}$ of the heat surface along the centerline of streamwise direction at Re = 200 situation are shown in Fig. 2. The definition of $Nu_{X_1}$ is shown as follows:

$$Nu_{X_1} = \frac{w_1}{k_0(T_h - T_0)}\left[k(T)\frac{\partial T}{\partial x_2}\right] \tag{27}$$

The deviations among the results are not apparent. The grid distribution of $200 \times 40 \times 40$ is then used. According to numerical tests, the related length variables are determined and shown as follows:

$$\begin{aligned} &w_2/w_1 = 1 \\ &w_3/w_1 = 0.05 \\ &h/w_1 = 0.175 \\ &l_1/w_1 = 15 \\ &l_2/w_1 = l_3/w_1 = 2.25 \\ &l_4/w_1 = 10.5 \end{aligned} \tag{28}$$

Due to the convenience of the computation of the immersed boundary, the computational time step is equal to the time of the block moving along one grid in $x_3$ direction which varies from 0.8 to 5 s accompanying with the variations of the Reynolds number and the velocity of the moving block. In one periodic movement 40 steps are necessary.

In Fig. 3, the results of velocities at the outlet of the channel are compared with the analytical solution [39] expressed in the following equation:

$$u_1(x_2, x_3) = \frac{4w_1^2}{\mu\pi^3}\left(-\frac{dp}{dx_1}\right)\sum_{i=1,3,5,\ldots}^{\infty}(-1)^{\frac{(i-1)}{2}}\left[1 - \frac{\cosh\left(\frac{i\pi x_3}{w_1}\right)}{\cosh\left(\frac{i\pi}{2w_1}\right)}\right] \times \frac{\cos\left(\frac{i\pi x_2}{w_1}\right)}{i^3} \tag{29}$$

In the central region, a slight difference exists between both results, and in the other regions. Both results have good agreements.

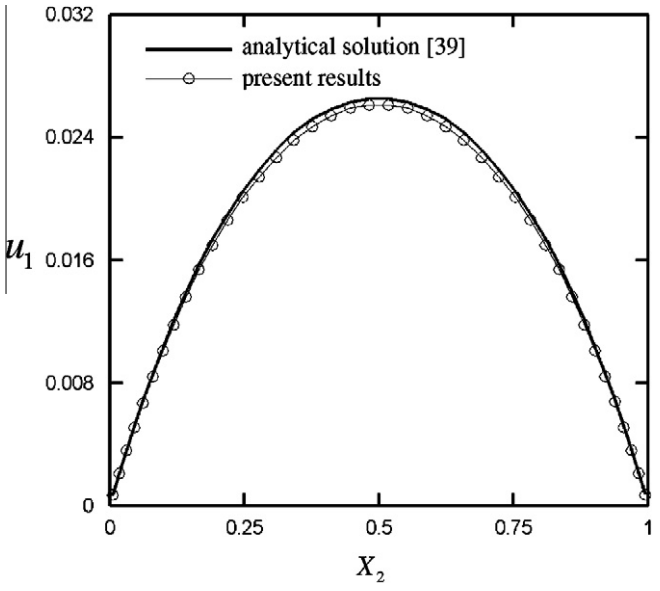


**Fig. 3.** Comparison of present results with analytical solution [39]. (Re = 600).

**Table 1**
Combinations of parameters of Reynolds number and velocity of slender block.

| | Re | Velocity of slender block ($V_b$) |
|---|---|---|
| Case1 | 200 | 1/4 |
| Case2 | 200 | 1/2 |
| Case3 | 600 | 1/4 |
| Case4 | 600 | 1/2 |

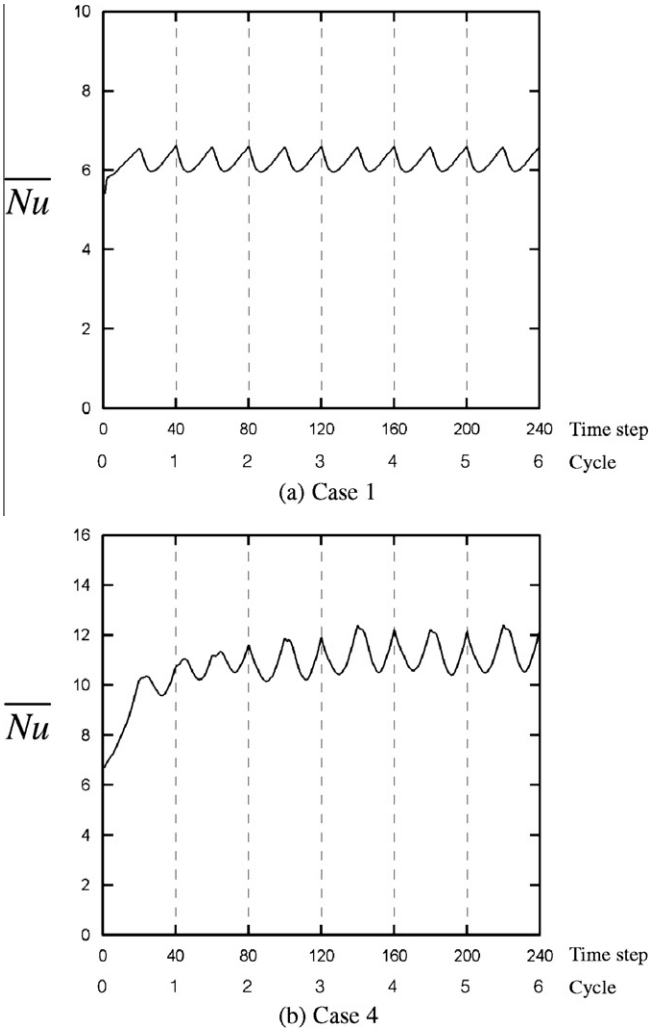


**Fig. 4.** Periodic variation of average Nusselt numbers of the heat surface in case 1 and case 4.

The situations investigated in the study are tabulated in Table 1. In Fig. 4, the variations of the average Nusselt numbers $\overline{Nu}$ from the beginning of movement of the slender block to several cycles are shown. The average Nusselt number $\overline{Nu}$ is defined in the following equation.

$$\overline{Nu} = \frac{1}{A}\int_{x_1}\int_{x_3} Nu_{x_3}\, dx_3\, dx_1 \tag{30}$$

where $A$ is the area of heat surface.

After three cycles, the steadily periodic variations of the average Nusselt numbers can be observed. The results indicated in the following paragraphs are under the steady periodic situation.

In Fig. 5a and b, the velocity fields on the $x_2x_3$ plane at the front (AB), and back (CD) cross sections which are shown in Fig. 1 under the situation of Re = 200 and $V_b$ = 1/4 are indicated, respectively. In

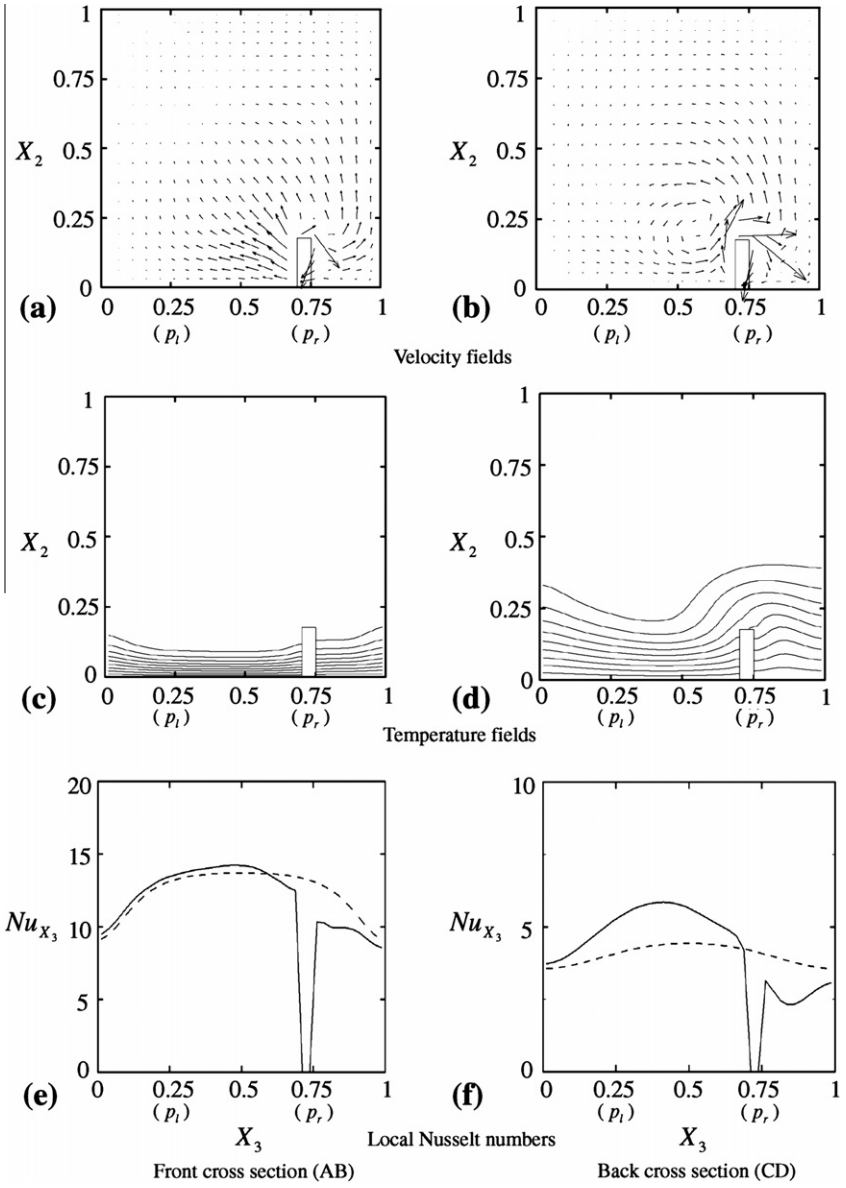


**Fig. 5.** Distributions of velocity, temperature and local Nusselt numbers of the front and back cross sections (Re = 200, $V_b$ = 1/4).

these figures, the slender block finishes its last periodic movement from the $p_l$ to $p_r$ position and just starts to execute a next new periodic movement from the $p_r$ to $p_l$ position. Shown in Fig. 5a, the channel flow impinges on the front edge of the slender block at all times. The velocities of fluids around the slender block are then immediately affected by the mutual effects of the channel flow and the movement of the block, and the velocity directions of fluids on the left side of the block are the same as that of the movement of the block itself. As for the behaviors of fluids on the narrow right side of the block, some fluids supplement vacant space caused by the movement of the block and flow behind the block, and some other fluids are suppressed by the channel flow and flow upward.

The velocity field on the back (CD) cross section is indicated in Fig. 5b. The cross section has certain distance away from the front edge of the heat surface, and for an instant the effect of the channel flow does not reach the cross section. Besides, the effect of the last periodic motion of the block still leaves, and fluids near the left side of the block then flow to the right side. The fluids near the right side of the block supplement vacant space caused by the movement of the block similar to that shown in Fig. 5a. A circulation induced by the interaction of the channel flow and the movement of the block is observed, and the behavior of circulation is like a rolling dish, and moves with the block closely.

Shown in Fig. 5c and d, the distributions of isothermal lines on the front and back cross sections which are separately corresponding to the cross sections indicated in Fig. 5a and b are indicated, respectively. In Fig. 5c, on the front cross section the channel flow which is not heated yet touches the heat surface first, the distribution of isothermal lines is naturally dense near the heat surface. The space on the right side of block is much narrower than that of the left side of block which causes the amount of fluids flowing through the space of the right side of block to be decreased. As a result, the distribution of isothermal lines of the right side of the block is sparser than that of the left side of the block.

Then in Fig. 5d, the distribution of isothermal lines of the back cross section which is located in the downstream region is sparser than that of the front cross section. Besides, the distribution of isothermal lines of the right side of the block is sparser than that of the left side of the block, and the reason is mentioned above. The behavior of circulation is like a rolling dish, then the distribution

of isothermal lines is suppressed by the circulation and a concave is found on the left side of block.

In Fig. 5e and f, the distributions of the local Nusselt numbers $Nu_{X_3}$ along the heat surfaces of the front and back cross sections are shown, respectively. The dashed lines indicate the situation without a moving block and the solid lines indicate the situation having a moving block. Shown in Fig. 5e, the channel flow first touches the heat surface at the front cross section that is very advantageous to the heat transfer rate of the heat surface. However, the moving velocity $V_b$ of the block in this case is relatively small which causes the promotion of the heat transfer rate of the heat surface to have limitation. Consequently, the local Nusselt numbers indicated by the solid line are slightly larger than those indicated by the dashed line in the left region of block. In the right region of the block, this region is narrow and less fluids flow through which leads the heat transfer rate of heat surface to get worse. Then in this region, the local Nusselt numbers indicated by the solid line are oppositely smaller than these indicated by the dashed line.

In Fig. 5f, the back cross section is farther away from the front edge of the heat surface, and the distribution of the local Nusselt numbers indicated by the dashed line on this cross section is naturally smaller than that of the front cross section. Due to the existence of circulation in the left region of the block, the thermal boundary layer of the heat surface is suppressed by the circulation that causes the local Nusselt numbers indicated by the solid line relative to those indicated by the dashed line to be enhanced and to become larger in magnitudes. In the narrow right region of the block, the mobility of fluid in this region is inferior and it is needless to say that the local Nusselt numbers indicated by the solid line are predictably smaller than those indicated by the dashed line.

In Fig. 6a and b, the block is moving to the center of heat surface, and the velocity fields on the front and back cross sections are indicated, respectively. A large and remarkable circulation zone is observed in each cross section, and the block is included in it. In the right bottom region of the block, due to the circulation, fluids flow quickly and close to the bottom surface. Those behaviors are

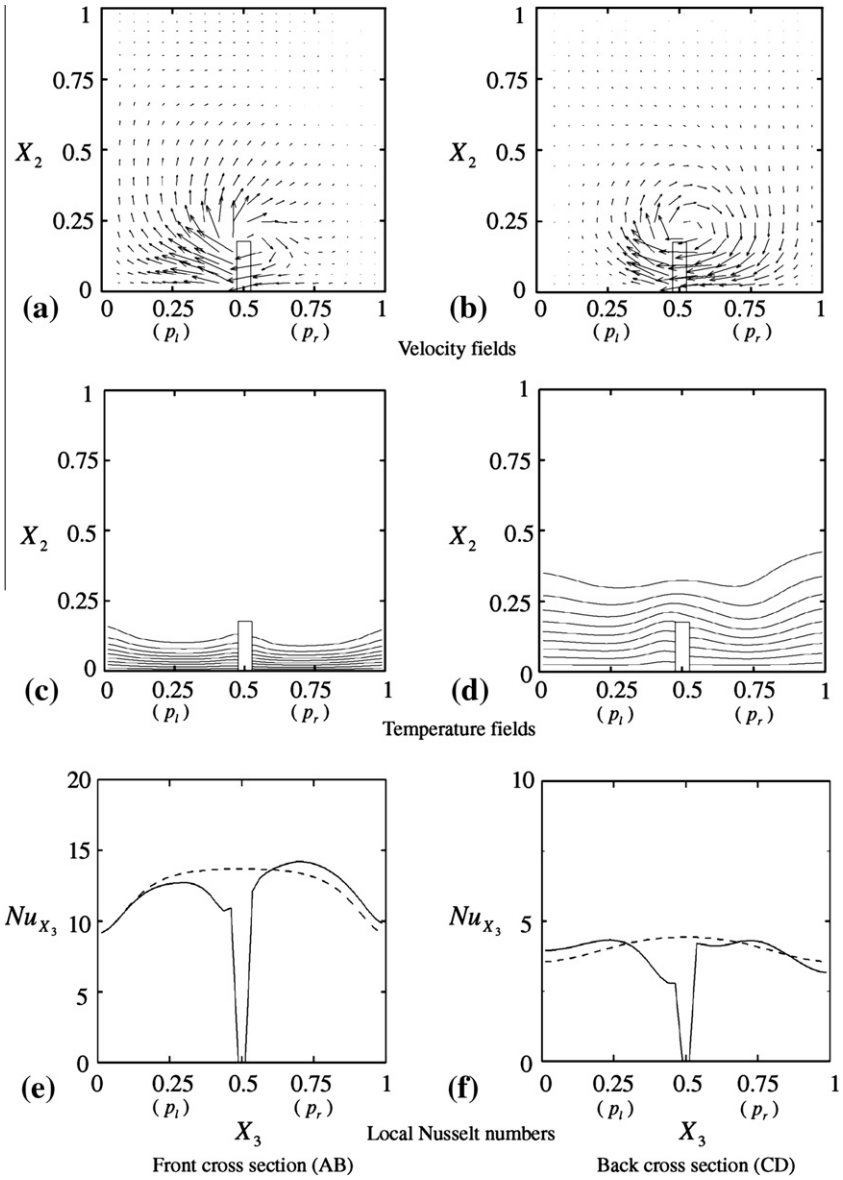


**Fig. 6.** Distributions of velocity, temperature and local Nusselt numbers of the front and back cross sections (Re = 200, $V_b$ = 1/4).

advantageous to the heat transfer rate of the heat surface. Due to the low velocities of the channel flow and the moving block, near the left bottom region of the block fluids are pushed forwards by the moving block, but the high-speed fluids don't flow close to the heat surface, and those behaviors are disadvantageous to the heat transfer rate of the heat surface.

Shown in Fig. 6c and d, the distributions of isothermal lines on the front and back cross sections are indicated, respectively. According to the descriptions of velocity fields mentioned above, in each cross section the distribution of isothermal lines in the right region of the block is denser than that in the opposite region. The movement of circulation follows the block tightly, and concaves on the distributions of isothermal lines indicated in those figures are not apparent.

In Fig. 6e and f, the distributions of local Nusselt numbers on the front and back cross sections are shown, respectively. Based on the distributions of isothermal lines mentioned above, in each cross section the local Nusselt numbers of the right region of the block are slightly larger than those of the opposite region. In the front zone of the moving block, the fluids flow upward which causes the local Nusselt numbers in this region to be inferior to those in the other region.

The magnitudes of the Reynolds number Re (=600) and the moving velocity of block $V_b$ (=1/2) of the following cases are the maximum values. The velocity fields shown in Fig. 7a and b are similar to those shown in Fig. 5a and b, respectively. Due to the more rapid velocities of the channel flow and the moving block, the interaction of both velocities becomes stronger which directly causes the distributions of isothermal lines of cross sections shown in Fig. 7 c and d to be denser than those shown in Fig. 5c and d. Therefore, the distributions of local Nusselt numbers indicated in Fig. 7e and f are then much different from those indicated in Fig. 5e and f. Relative to the case without a moving block (dashed line), the local Nusselt numbers shown in those figures are enhanced far and wide on each cross section.

Shown in Fig. 8a and b the block moves to the center of the cross section. Around the block, high-speed fluids flow close to the bottom surface which is helpful to suppress the boundary layer of the heat surface and to enhance the heat transfer rate of the heat surface. Then the variations of the distributions of isothermal lines

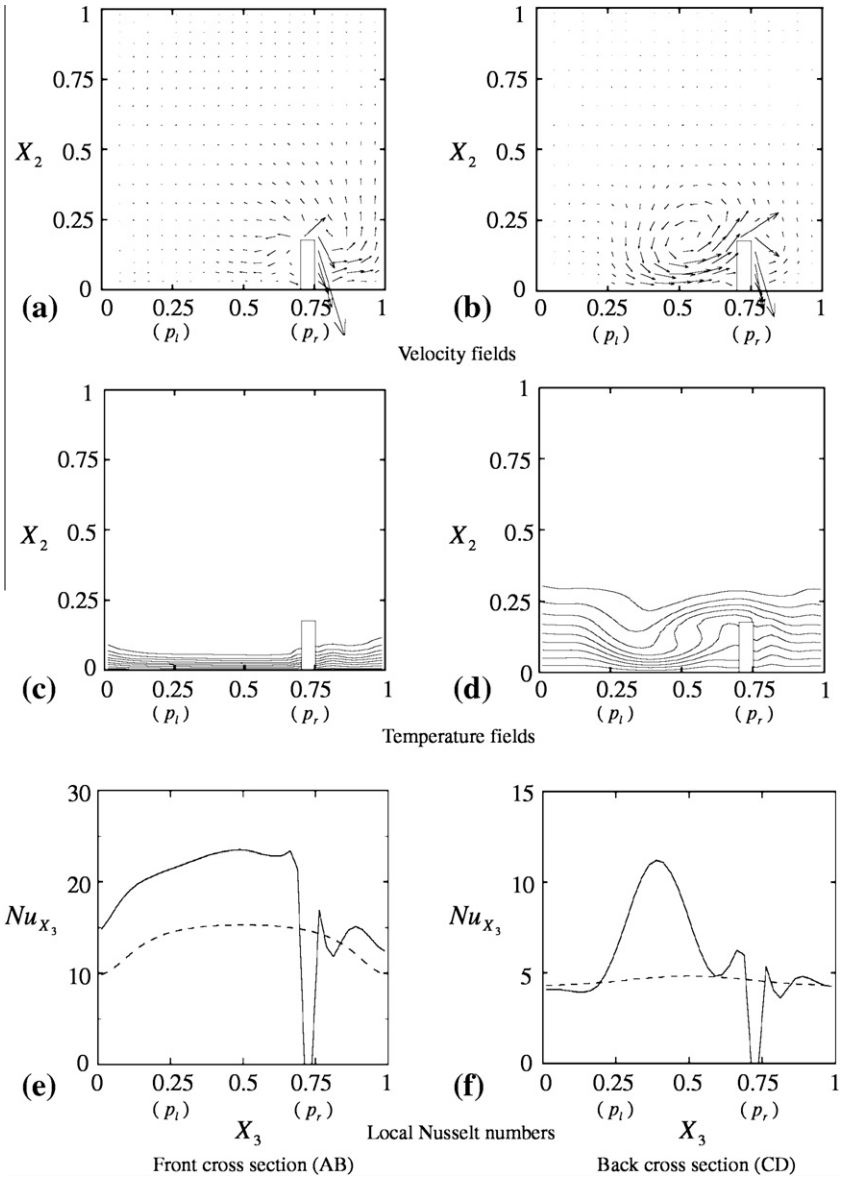


**Fig. 7.** Distributions of velocity, temperature and local Nusselt numbers of the front and back cross sections (Re = 600, $V_b$ = 1/2).

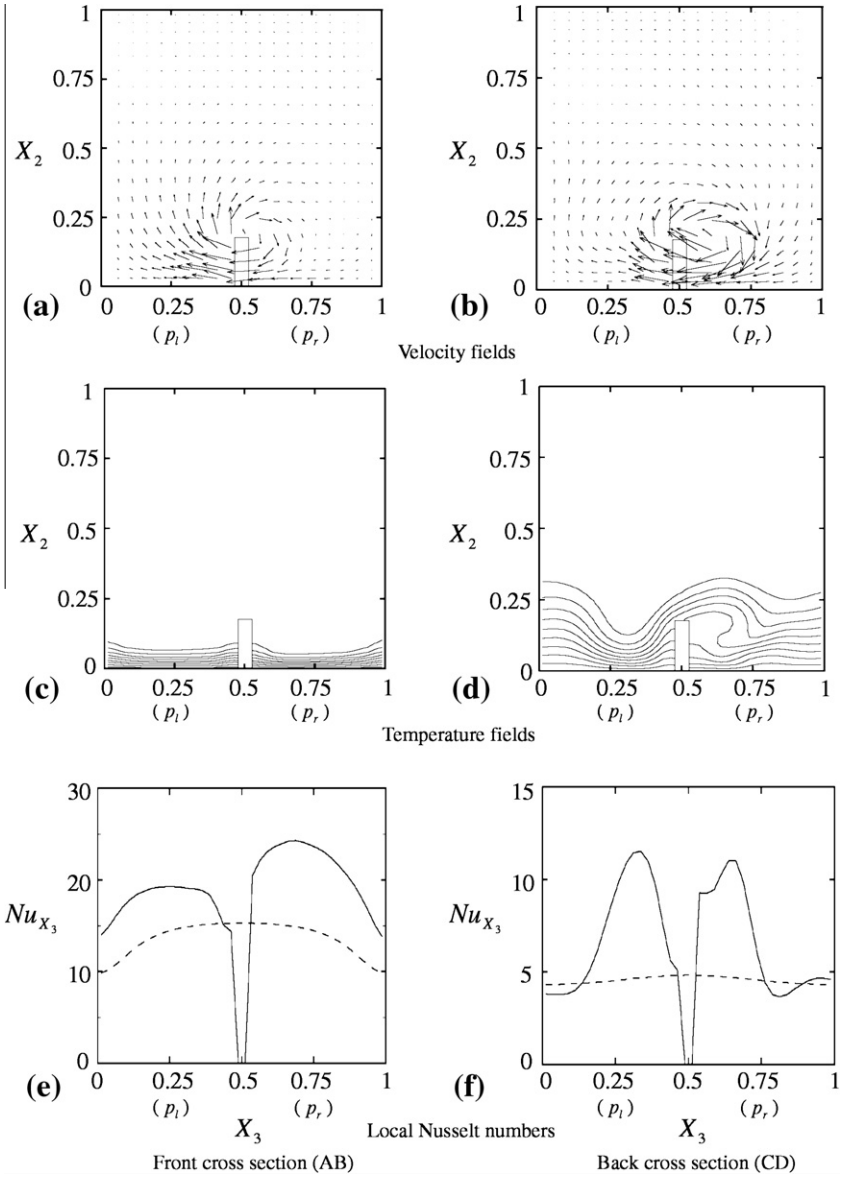


**Fig. 8.** Distributions of velocity, temperature and local Nusselt numbers of the front and back cross sections (Re = 600, $V_b = 1/2$).

shown in Fig. 8c and d are more drastic than those shown in Fig. 6c and d. Shown in Fig. 8e, based upon the results mentioned above even on the front edge cross section the local Nusselt numbers indicated by solid line are apparently larger than those indicated by dashed line. Similarly, on the back cross section Fig. 8f the local Nusselt numbers indicated by solid line are still larger than those indicated by dashed line. The enhancement of the heat transfer rates of less-efficient regions can be improved by this method.

In Fig. 9a and b, comparisons of the average local Nusselt numbers of the heat surface along the centerline of streamwise direction at Re = 200 and 600 situations are indicated, respectively. The definition of the average local Nusselt number of $\overline{Nu}_{x_1}$ is expressed as follows:

$$\overline{Nu}_{x_1} = \frac{1}{t_p}\int_t Nu_{x_1}\,dt, \quad t_p = \text{time of a cycle} \tag{31}$$

Due to the slow velocities of channel flow and moving slender block, the effect of interaction between both velocities on the heat transfer rate is weak, then the enhancement of the heat transfer rate is difficult to achieve on the whole heat surface.

Relative to the results shown in Fig. 9a, in Fig. 9b both velocities of channel flow and the moving slender block are quicker which causes the effect of interaction between both velocities on the heat transfer rate to become strong. As a result, the enhancement of the heat transfer rate is achieved in the whole region.

Enhancement of the average heat transfer rate of the heat surface of a cycle *En* tabulated in Table 2 is calculated by the following equation:

$$En = \frac{(Nu)_{with\ block} - (Nu)_{without\ block}}{(Nu)_{without\ block}} \tag{32}$$

where $(Nu) = \frac{1}{t_p}\int_t \overline{Nu}dt$, $t_p$ = time of a cycle.

Since the interaction of the velocities of channel flow and the moving block is strong under high Reynolds number situations, the strong interaction directly causes the heat transfer rate to increase and remarkable enhancements of the heat transfer rate are achieved. Oppositely, under low Reynolds number situations, the effect of interaction is worse and becomes a burden for favorable fluid flows of heat transfer, and then the enhancements of heat transfer are inferior.

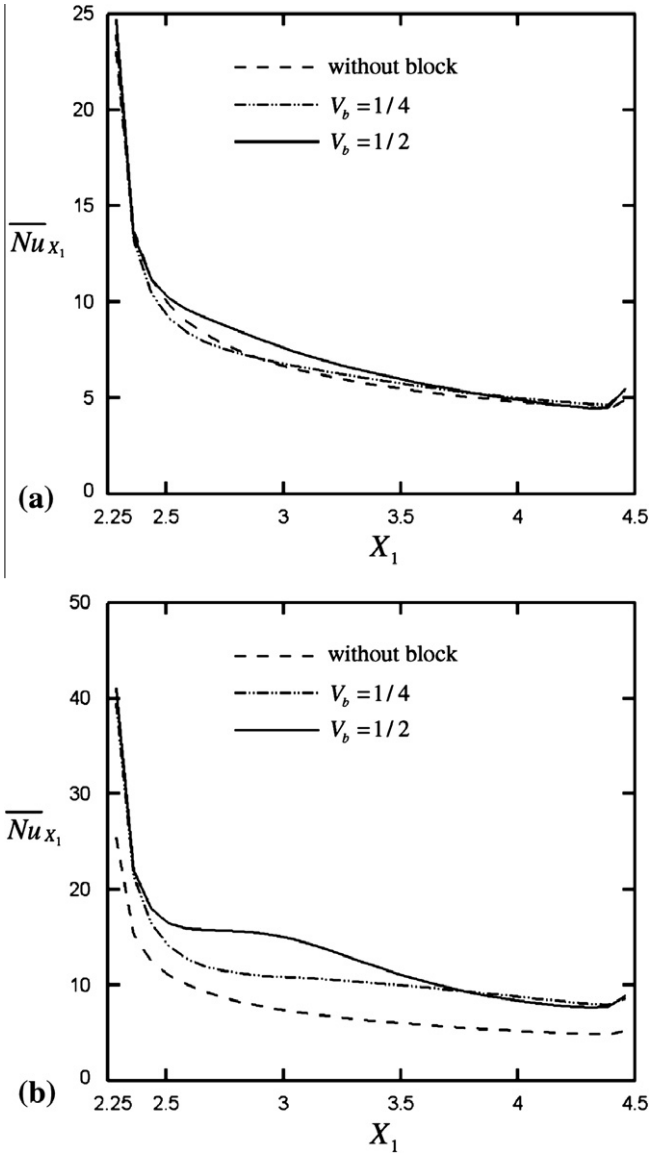


**Fig. 9.** Comparisons of the average local Nusselt numbers of heat surface along the centerline of streamwise direction.

**Table 2**
Enhancement of heat transfer rate of a cycle *En*.

| Re | $V_b$ | *Nu* | *En* (%) |
|---|---|---|---|
| 200 | N/A | 6.31 | N/A |
| 200 | 1/4 | 6.22 | −1.42 |
| 200 | 1/2 | 6.51 | 3.11 |
| 600 | N/A | 7.03 | N/A |
| 600 | 1/4 | 10.02 | 42.40 |
| 600 | 1/2 | 10.84 | 54.04 |

## 5. Conclusions

Enhancement of heat transfer rate of a channel flow with insertion of a moving slender block is investigated. Several conclusions are summarized as follows:

(1) Achievement of using a moving block to enhance heat transfer rate of a channel flow is remarkable especially in the downstream of channel flow.
(2) Behaviors of the moving block and the rolling circulation induced by the interaction between the motions of channel flow and moving block play an important role in enhancing heat transfer rate of a channel flow.
(3) A case of low velocities of channel flow and moving block is a counter-effect for promotion of the heat transfer rate of channel flow.

## Acknowledgements

The authors gratefully acknowledge the support of the Natural Science Council, Taiwan, ROC under Contact NSC96-2221-E-009-059 and National Center for High-Performance Computing of Taiwan, ROC.

## References

[1] A.E. Bergles, Recent development in convective heat transfer augmentation, Appl. Mech. Rev. 26 (1973) 675–682.
[2] A.E. Bergles, Survey and evaluation of techniques to augment convective heat and mass transfer, Heat Mass Transfer 1 (1969) 331–424.
[3] H.W. Markstein, New development in cooling techniques, Electron, Packaging Prod. 16 (1975) 36–44.
[4] S. Sathe, K.M. Karki, C. Tai, C. Lamb, S.V. Patanker, Numerical prediction of flow and heat transfer in an impingement heat sink, J. Electron. Packaging 119 (1997) 58–63.
[5] Y. Kondo, M. Behnia, W. Nakayama, H. Matsushima, Optimization of finned jet sinks for impingement cooling of electronic packages, J. Electron. Packaging 120 (1998) 259–266.
[6] K. Vafai, Z. Lu, Analysis of two-layered micro-channel heat sink concept in electronic cooling, Int. J. Heat Mass Transfer 42 (1999) 2287–2297.
[7] X. Chen, W.H. Sutton, Enhancement of heat transfer: combined convection and radiation in the entrance region of circular ducts with porous inserts, Int. J. Heat Mass Transfer 48 (2005) 5460–5474.
[8] N. Yucel, R.T. Guven, Forced-convection cooling enhancement of heated elements in a parallel-plate channels using porous inserts, Numer. Heat Transfer A 51 (2007) 293–312.
[9] M. Gharebaghi, I. Sezai, Enhancement of heat transfer in latent heat storage modules with internal fins, Numer. Heat Transfer A 53 (2008) 749–765.
[10] Y. Zeng, K. Vafai, An investigation of convective cooling of an array of channel-mounted obstacles, Numer. Heat Transfer A 55 (2009) 967–982.
[11] P. Parthasarathy, P. Talukdar, V.R. Kishore, Enhancement of heat transfer with porous/solid insert for laminar flow of a participating gas in a 3-D square duct, Numer. Heat Transfer A 56 (2009) 764–784.
[12] Y. Tanida, A. Okaijma, Y. Watanabe, Stability of a circular cylinder oscillating an uniform flow, J. Fluid Mech. 61 (1973) 769–784.
[13] S.E. Hurlbut, M.L. Spaulding, F.M. White, Numerical solution for laminar two dimensional flow about a cylinder oscillating in a uniform stream, J. Fluids Eng. 104 (1982) 217–222.
[14] R. Chilukuri, Incompressible laminar flow pass a transversely vibrating cylinder, J. Fluids Eng. 109 (1987) 166–171.
[15] M.O. Griffin, M.S. Hall, Review-vortex shedding lock-on and flow control in bluff body wakes, J. Fluids Eng. 113 (1991) 526–567.
[16] J. Zhang, C. Dalton, Interaction of a steady approach flow and a circular cylinder undergoing forced oscillation, J. Fluids Eng. 119 (1997) 808–813.
[17] C. Zhu, H. Liang, D. Sun, L. Wang, Y. Zhang, Numerical study of interactions of vortices generated by vortex generators and their effects on heat transfer enhancement, Numer. Heat Transfer A 50 (2006) 345–360.
[18] S. Jayavel, S. Tiwari, Numerical study of flow and heat transfer for flow past inline circular tubes built in a rectangular channel in the presence of vortex generators, Numer. Heat Transfer A 54 (2008) 777–797.
[19] Y.Y. Chen, K.W. Song, L.B. Wang, D.L. Sun, Comparisons of local experimental results of heat transfer enhancement of a flat tube bank fun with vortex generators, Numer. Heat Transfer A 55 (2009) 144–162.
[20] H. Ishida, H. Kimoto, The structures of attractors reconstructed with time-evolution data of average heat transfer on thermal convection field in a vibrating square enclosure, Heat Transfer Asian Res. 30 (1) (2001) 11–21.
[21] R.E. Forbes, C.T. Carley, C.J. Bell, Vibration effects on convective heat transfer in enclosure, J. Heat Transfer – Trans. ASME (1970) 429–438.
[22] C.B. Baxi, A. Ramachandran, Effect of vibration on heat transfer from spheres, J. Heat Transfer – Trans. ASME (1969) 337–344.
[23] K.N. Krishnan, B.K. Subba Rao, Effect of vibration on the performance of a double pipe heat exchanger, Indian J. Technol. 13 (1975) 1–5.
[24] W.S. Fu, B.H. Tong, Numerical investigation of heat transfer from a heated oscillating cylinder in a cross flow, Int. J. Heat Mass Transfer 45 (2002) 3033–3043.
[25] W.S. Fu, B.H. Tong, Numerical investigation of heat transfer characteristics of the heated blocks in the channel with a transversely oscillating cylinder, Int. J. Heat Mass Transfer 47 (2004) 341–351.

[26] J. Li, Numerical approximation of unsteady natural convection from a vertical flat plate with a surface temperature oscillation, Numer. Heat Transfer A 46 (2004) 383–399.
[27] W.S. Fu, K.N. Wang, An investigation of a block moving back and forth on a heat plate under a slot jet, Int. J. Heat Mass Transfer 44 (2001) 2621–2631.
[28] W.S. Fu, C.C. Tseng, K.N. Wang, C.P. Huang, An experimental investigation of a block moving back and forth on a heat plate under a slot jet, Int. J. Heat Mass Transfer 50 (2007) 3224–3233.
[29] C.S. Peskin, Flow patterns around heart valves: a numerical method, J. Comput. Phys. 10 (1972) 252–271.
[30] T.B. Trong, A parallel finite-volume algorithm for large-eddy simulation of turbulence flows, Comput. Fluids 29 (2000) 877–915.
[31] P.L. Roe, Approximation Riemann solver, parameter vectors, and difference schemes, J. Comput. Phys. 43 (1981) 357–372.
[32] J.M. Weiss, W.A. Smith, Preconditioning applied to variable and constants density flows, AIAA 33 (1995) 2050–2056.
[33] J. Dennis, P. Thomas, B. Pieter, Recent enhancements to OVERFLOW, in: 35th Aerospace Sciences Meeting and Exhibit, Reno, NV, 1997.
[34] S. Yoon, S. Jameson, Lower-upper symmetric-Gauss–Seidel method for the Euler and Navier–Stokes equations, AIAA 26 (1988) 1025–1026.
[35] I. Abalakin, A. Dervieux, T. Kozubskaya, A vertex centered high order MUSCL scheme applying to linearized Euler acoustics, INRIA (2002) 4459.
[36] R. Verzicco, J. Mohd-Yusof, P. Orlandi, D. Haworth, Les in complex geometries using boundary body forces, AIAA 38 (2000) 427–433.
[37] D.G.E. Grigoriadis, J.G. Bartzis, A. Goulas, LES of the flow past a rectangular cylinder using a immersed boundary concept, Int. J. Numer. Methods Fluids 41 (2003) 615–632.
[38] C.W. Li, L.L. Wang, An immersed boundary finite difference method for LES of flow around bluff shapes, Int. J. Numer. Methods Fluids 46 (2004) 85–107.
[39] F.M. White, Viscous Fluid Flow, McGrawHill Co., Ltd., 2006. p. 113.